Journal of Zhejiang University-SCIENCE C (Computers & Electronics)
ISSN 1869-1951 (Print); ISSN 1869-196X (Online)
www.zju.edu.cn/jzus; www.springerlink.com
E-mail: jzus@zju.edu.cn

Interconnection and damping assignment and Euler-Lagrange passivity-based control of photovoltaic/battery hybrid power source for stand-alone applications*

Ali TOFIGHI[1,2], Mohsen KALANTAR[2]

([1]*Department of Electrical Engineering, Pardis Branch, Islamic Azad University, Pardis, Iran*)

([2]*Center of Excellence for Power System Automation and Operation, Department of Electrical Engineering, Iran University of Science and Technology, Tehran, Iran*)

E-mail: {tofighi, kalantar}@iust.ac.ir

Received Oct. 21, 2010; Revision accepted Jan. 25, 2011; Crosschecked July 29, 2011

Abstract: A DC hybrid power source composed of photovoltaic cells as the main power source, Li-ion battery storage as the secondary power source, and power electronic interface, is modeled based on port-controlled Hamiltonian systems and Euler-Lagrange framework. Subsequently, passivity-based controllers are synthesized. Local asymptotic stability is ensured as well. In addition, a power management system is designed to manage power flow between components. Modeling and simulation of the proposed hybrid power source is accomplished using MATLAB/Simulink. Our interest is focused on the comparison of the two passivity-based control methods and their use in hybrid power systems.

Key words: DC hybrid power source, Euler-Lagrange (EL) equations, Interconnection and damping assignment (IDA), Passivity-based control, Photovoltaic, Li-ion battery

doi:10.1631/jzus.C1000368 **Document code:** A **CLC number:** TP274; TM911.4

1 Introduction

Renewable energy resources are desirable for electrical power generation due to their environmentally-friendly nature. Among the renewable energy resources, solar energy is now widely used because it is free, abundant, and pollution-free (Kwon *et al*., 2006).

It is estimated that about 80% of all photovoltaic (PV) systems are used in stand-alone applications (Duryea *et al*., 2001). Furthermore, the generated power of the PV system depends on weather conditions. For example, during cloudy periods, and at night, a PV system would not generate any power (Yu and Yuvarajan, 2006). Hence, hybrid power sources are introduced to make the best use of solar energy (Lu and Agelidis, 2009; Dali *et al*., 2010). Batteries are a secondary source which stores solar energy and is used when needed under hybrid system constraints (Glavin *et al*., 2008; Golkar and Hajizadeh, 2009; Lagorse *et al*., 2009).

Power electronic converters play a significant role in the hybrid systems (Carrasco *et al*., 2006). These are interfaced between the distributed generation (DG) sources and the other parts of the hybrid system (Lagorse *et al*., 2009). Recently, some researchers have concerned themselves with the control of hybrid power sources (El-Shatter *et al*., 2006; Moreno *et al*., 2006; Jiang *et al*., 2007). The methods of controller design are classified into two categories: linear and nonlinear. The linear methods are performed with a reliance on locally-linearized models. Hence, their performance will not remain the same under changes to any of the equilibrium points. The

* Project supported by Iran University of Science and Technology, Iran

proportional-integral (PI) controller is a main linear controller which is being used in DG applications (Kwon *et al*., 2008; Wang and Chang, 2008; Timbus *et al*., 2009; Uzunoglu *et al*., 2009). The dynamic equations of the power electronic converters have a nonlinear nature due to the multiplications of the state variables by the control inputs (Sira-Ramirez *et al*., 1998). Therefore, the nonlinear methods such as robust (Mazumder *et al*., 2002), feedback linearization (Kim and Lee, 2007), sliding mode (Vmquez *et al*., 2003), and passivity-based (Leyva *et al*., 2006) control are used for control of converters. In particular, a passivity-based control (PBC) method is taken into consideration in various industrial applications.

PBC was introduced by Ortega *et al.* (2002) as a controller design methodology which achieves stabilization by passivation. Two theories for PBC were developed: Euler-Lagrange (EL) PBC (Ortega *et al*., 1998; Scherpen *et al*., 2003) and interconnection and damping assignment (IDA) PBC (Ortega *et al*., 2002). These methods have been used mostly for control of induction motors (Dòria-Cerezo, 2006) and switching power converters (Kwasinski and Krein, 2007; Wang *et al*., 2008).

Lee (2004) has used EL-PBC for control of three-phase AC/DC voltage source converters. Also, a single-phase pulse width modulated (PWM) current source inverter control with applying IDA-PBC has been implemented by Komurcugil (2010). The control of a fuel cell/ultracapacitor hybrid system has been achieved based on IDA-PBC by Ayad *et al*. (2010). Becherif *et al.* (2007) used IDA-PBC for energy management of the solar energy system and battery.

This paper is concentrated on the port-controlled Hamiltonian form and Lagrangian modeling of PV/battery stand-alone hybrid power source. PV system is the main power source. Whenever the generated power of PV, with consideration of weather conditions, is less than the load power, the battery storage is used as a secondary power source. The dump load consumes the excess power of the PV system whenever the generated power is more than the load power, and the battery storage does not need to charge. The control signals are achieved by PBC. Power flow between hybrid system components is managed in the power management unit.

2 The proposed system description

The proposed hybrid power source is depicted in Fig. 1. This power source consists of a PV system, Li-ion battery storage, DC/DC converters, and load.

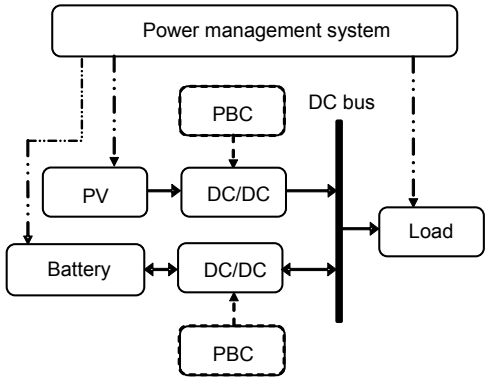

Fig. 1 Structure of the proposed hybrid DC power source
PBC: passivity-based control; PV: photovoltaic

2.1 Solar energy system

A solar cell is the fundamental component of a PV system, which converts the solar energy into electrical energy. A solar cell consists of a p–n junction semiconductor material. A PV panel consists of a certain number of solar cells connected in series/parallel combination to provide the desired voltage and current. A PV array consists of a number of panels connected in series/parallel combination (Kim *et al*., 2006). The equivalent circuit of a solar cell is depicted in Fig. 2.

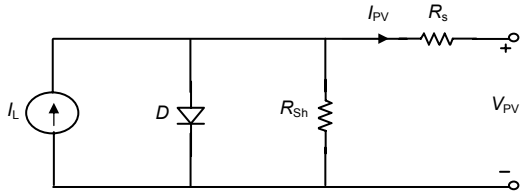

Fig. 2 Solar cell equivalent circuit

The circuit mainly consists of a current source I_L whose amplitude depends on irradiance and temperature, a diode D, and internal shunt and series resistances R_{Sh}, R_s. The *V-I* characteristic of the solar cell is highly nonlinear, given by the following equation:

$$I_{PV} = I_L - I_0\left[\exp\left(\frac{q(V_{PV}+R_sI_{PV})}{AKT}\right)-1\right]-\frac{V_{PV}+I_{PV}R_s}{R_{Sh}}, \quad (1)$$

where V_{PV} and I_{PV} are the solar cell voltage and current respectively, I_0 is the diode reverse saturation current, q is the electron charge, A is the ideality factor of the p–n junction, K is Boltzman's constant, and T is the cell temperature (Koutroulis *et al*., 2001).

The power delivered by the PV module depends on the solar irradiance, cell temperature, efficiencies of the system components, etc. Thus, it is necessary that the maximum power be drawn in different conditions. The usual approach for maximizing the power drawn from PV arrays under varying atmospheric conditions is to use a maximum power point tracker (MPPT) algorithm that provides a reference voltage or current for the DC/DC converter (Scarpa *et al*., 2009). Several techniques for MPPT have been presented in the literature (Esram and Chapman, 2007).

In this study, the maximum power is drawn from PV arrays with implementation of the perturbation and observation (P&O) method (Sera *et al*., 2006).

2.2 Lithium-ion battery model

Storage devices are used as energy storing in the hybrid power sources (Jeong *et al*., 2005; Khateeb *et al*., 2006). The batteries store energy in the electrochemical form. Li-ion batteries are preferable to other types of batteries because they have high energy density, high operating voltage levels, and long cycle life (Durr *et al*., 2006).

In this section, the dynamic model of Li-ion battery is introduced which is used in the simulation program. Chen and Rincon-Mora (2006) proposed a suitable model for Li-ion battery which accurately predicts battery runtime and *I-V* performance. The aforementioned model of the Li-ion battery is depicted in Fig. 3.

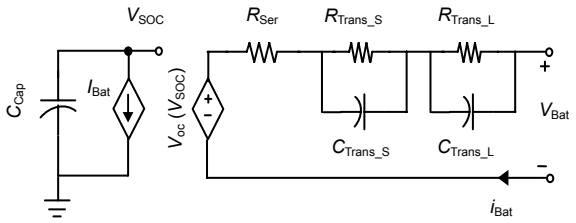

Fig. 3 Li-ion battery electrical circuit model

The model consists of two separate circuits linked by a voltage-controlled voltage source and a current-controlled current source. The runtime and state of charge (SOC) of the battery are calculated using the left side circuit. The equivalent internal impedance simulates the internal resistance and transient behavior of the battery. Hence, R_{Ser} is responsible for voltage drop in battery voltage, and the components of the RC networks are responsible for short- and long-time transients in the battery internal impedance. The elements of the equivalent internal impedance are a function of SOC, and can be achieved as

$$\begin{cases} R_{Ser}(\mathrm{SOC}) = 0.1562\mathrm{e}^{-24.375\mathrm{SOC}} + 0.07446, \\ R_{Trans\_S}(\mathrm{SOC}) = 0.3208\mathrm{e}^{-29.14\mathrm{SOC}} + 0.04669, \\ C_{Trans\_S}(\mathrm{SOC}) = -752.9\mathrm{e}^{-13.51\mathrm{SOC}} + 703.6, \\ R_{Trans\_L}(\mathrm{SOC}) = 6.603\mathrm{e}^{-155.2\mathrm{SOC}} + 0.04984, \\ C_{Trans\_L}(\mathrm{SOC}) = -6056\mathrm{e}^{-27.12\mathrm{SOC}} + 4475, \\ V_{OC}(\mathrm{SOC}) = -1.031\mathrm{e}^{-35\mathrm{SOC}} + 3.685 + 0.2156\mathrm{SOC} \\ \qquad\qquad - 0.1178\mathrm{SOC}^2 + 0.3201\mathrm{SOC}^3, \\ \mathrm{SOC}(t) = \mathrm{SOC}(0) - \dfrac{1}{C_{Cap}}\int_0^t i(\tau)\mathrm{d}\tau. \end{cases} \quad (2)$$

2.3 DC/DC converter

The amplitude of DC output voltage of the PV system depends on the solar irradiance delivered to PV arrays. Therefore, the boost DC/DC converter is used to adjust the output voltage of the PV system. Also, a bidirectional DC/DC converter is used to control the charging and discharging of the battery storage. The boost DC/DC converters are depicted in Fig. 4.

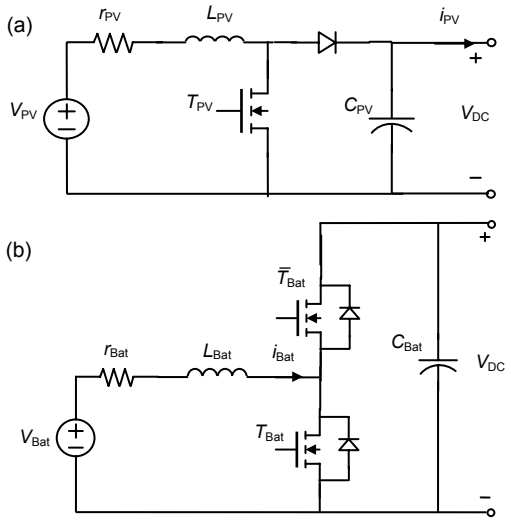

Fig. 4 Boost DC/DC converters: (a) unidirectional; (b) bidirectional

3 Port controlled Hamiltonian model

Port controlled Hamiltonian (PCH) systems were introduced by Dalsmo and van der Schaft (1998) for network modeling of lumped-parameter physical systems with independent storage elements (Ortega *et al*., 2002).

Consider the nonlinear system given by

$$\dot{\boldsymbol{x}} = f(\boldsymbol{x}) + g(\boldsymbol{x})\boldsymbol{u}, \tag{3}$$

where $\boldsymbol{x}\in\mathbb{R}^n$ is the state vector, $f(\boldsymbol{x})$ and $g(\boldsymbol{x})$ are locally Lipschitz functions, and $\boldsymbol{u}\in\mathbb{R}^m$ is the control input. The PCH form of Eq. (3) is (Ortega *et al*., 2002)

$$\begin{cases} \dot{\boldsymbol{x}} = \big(\boldsymbol{J}(\boldsymbol{x}) - \boldsymbol{R}(\boldsymbol{x})\big)\dfrac{\partial H(\boldsymbol{x})}{\partial \boldsymbol{x}} + g(\boldsymbol{x})\boldsymbol{u}, \\ \boldsymbol{y} = g(\boldsymbol{x})^{\mathrm{T}}\dfrac{\partial H(\boldsymbol{x})}{\partial \boldsymbol{x}}, \end{cases} \tag{4}$$

where $H(\boldsymbol{x})$: $\mathbb{R}^n\to\mathbb{R}$ is the energy (or Hamiltonian) function, $\boldsymbol{J}(\boldsymbol{x})=-\boldsymbol{J}(\boldsymbol{x})^{\mathrm{T}}\in\mathbb{R}^{n\times m}$ is the interconnection structure matrix, and $\boldsymbol{R}=\boldsymbol{R}^{\mathrm{T}}\geq\boldsymbol{0}\in\mathbb{R}^{n\times m}$ is the dissipation matrix.

The energy-balancing, passivity, and stabilization of the PCH system have been discussed by Ortega *et al.* (2002). Also, to solve the passivation problem they proposed the IDA-PBC methodology.

3.1 IDA-PB controller design

The main idea of IDA-PBC is to assign the desired closed-loop energy function via the modification of the interconnection and dissipation matrices (Wang *et al*., 2008). Therefore, a PCH system with consideration of desired target dynamic is of the following form:

$$\dot{\boldsymbol{x}} = \big(\boldsymbol{J}_{\mathrm{d}}(\boldsymbol{x}) - \boldsymbol{R}_{\mathrm{d}}(\boldsymbol{x})\big)\frac{\partial H_{\mathrm{d}}(\boldsymbol{x})}{\partial \boldsymbol{x}}, \tag{5}$$

where $H_{\mathrm{d}}(\boldsymbol{x})=H(\boldsymbol{x})+H_{\mathrm{a}}(\boldsymbol{x})$ is a new energy function that has a strict local minimum at the equilibrium $\boldsymbol{x}_{\mathrm{d}}$, and $\boldsymbol{J}_{\mathrm{d}}(\boldsymbol{x}) = -\boldsymbol{J}_{\mathrm{d}}(\boldsymbol{x})^{\mathrm{T}}$ and $\boldsymbol{R}_{\mathrm{d}}(\boldsymbol{x}) = \boldsymbol{R}_{\mathrm{d}}(\boldsymbol{x})^{\mathrm{T}}$ are targeting interconnection and damping matrices, respectively.

The partial derivative equation (PDE) with chosen matrices $\boldsymbol{J}_{\mathrm{d}}(\boldsymbol{x})$, $\boldsymbol{R}_{\mathrm{d}}(\boldsymbol{x})$ and a vector function $\boldsymbol{K}(\boldsymbol{x}) = \dfrac{\partial H_{\mathrm{a}}(\boldsymbol{x}_{\mathrm{d}})}{\partial \boldsymbol{x}}$ will be satisfied as

$$\begin{aligned} &\big(\boldsymbol{J}(\boldsymbol{x},\boldsymbol{u}) - \boldsymbol{R}(\boldsymbol{x})\big)\frac{\partial H(\boldsymbol{x})}{\partial \boldsymbol{x}} + g(\boldsymbol{x})\boldsymbol{u} \\ &\qquad = \big(\boldsymbol{J}_{\mathrm{d}}(\boldsymbol{x}) - \boldsymbol{R}_{\mathrm{d}}(\boldsymbol{x})\big)\frac{\partial H_{\mathrm{d}}(\boldsymbol{x})}{\partial \boldsymbol{x}}, \end{aligned} \tag{6}$$

such that (Ortega *et al*., 2002; Márquez-Contreras *et al*., 2008):

(i) (Structure preservation)

$$\begin{cases} \boldsymbol{J}_{\mathrm{d}}(\boldsymbol{x}) = \boldsymbol{J}(\boldsymbol{x},\boldsymbol{u}) + \boldsymbol{J}_{\mathrm{a}}(\boldsymbol{x}) = -\big(\boldsymbol{J}(\boldsymbol{x},\boldsymbol{u}) + \boldsymbol{J}_{\mathrm{a}}(\boldsymbol{x})\big)^{\mathrm{T}}, \\ \boldsymbol{R}_{\mathrm{d}}(\boldsymbol{x}) = \boldsymbol{R}(\boldsymbol{x}) + \boldsymbol{R}_{\mathrm{a}}(\boldsymbol{x}) = \big(\boldsymbol{R}(\boldsymbol{x}) + \boldsymbol{R}_{\mathrm{a}}(\boldsymbol{x})\big)^{\mathrm{T}} \geq \boldsymbol{0}. \end{cases} \tag{7}$$

(ii) (Integrability) $\boldsymbol{K}(\boldsymbol{x})$ is the gradient of a scalar function:

$$\frac{\partial \boldsymbol{K}(\boldsymbol{x})}{\partial \boldsymbol{x}} = \left(\frac{\partial \boldsymbol{K}(\boldsymbol{x})}{\partial \boldsymbol{x}}\right)^{\mathrm{T}}. \tag{8}$$

(iii) (Equilibrium assignment) when $\boldsymbol{x}=\boldsymbol{x}_{\mathrm{d}}$,

$$\left.\frac{\partial H_{\mathrm{d}}}{\partial \boldsymbol{x}}\right|_{\boldsymbol{x}=\boldsymbol{x}_{\mathrm{d}}} = \left.\left(\frac{\partial H}{\partial \boldsymbol{x}} + \frac{\partial H_{\mathrm{a}}}{\partial \boldsymbol{x}}\right)\right|_{\boldsymbol{x}=\boldsymbol{x}_{\mathrm{d}}} = \boldsymbol{0}. \tag{9}$$

(iv) (Lyapunov stability)

$$\left.\frac{\partial^2 H_{\mathrm{d}}}{\partial \boldsymbol{x}^2}\right|_{\boldsymbol{x}=\boldsymbol{x}_{\mathrm{d}}} > \boldsymbol{0}. \tag{10}$$

4 Euler-Lagrange model of the hybrid power source

In previous sections, a suitable model for DC/DC converters and other components have been presented. In this section, their EL description is expressed.

The Lagrangian $L(\dot{\boldsymbol{q}},\boldsymbol{q})$ of the system is the difference of the magnetic co-energy of the inductive elements, denoted by $T(\dot{\boldsymbol{q}},\boldsymbol{q})$, and the electric field energy of the capacitive elements, denoted by $V(\boldsymbol{q})$, i.e.,

$$L(\dot{\boldsymbol{q}},\boldsymbol{q}) = T(\dot{\boldsymbol{q}},\boldsymbol{q}) - V(\boldsymbol{q}), \tag{11}$$

where $\boldsymbol{q}$ is the vector of the electric charges and $\dot{\boldsymbol{q}}$ is the vector of the flowing current. The EL modeling equations with consideration of circuit constraints is (Scherpen *et al*., 2003)

$$\begin{aligned}\frac{\mathrm{d}}{\mathrm{d}t}\left(\frac{\partial L(\dot{\boldsymbol{q}},\boldsymbol{q})}{\partial \dot{\boldsymbol{q}}}\right)-\frac{\partial L(\dot{\boldsymbol{q}},\boldsymbol{q})}{\partial \boldsymbol{q}}&=-\frac{\partial D(\dot{\boldsymbol{q}})}{\partial \dot{\boldsymbol{q}}}+\boldsymbol{A}(\boldsymbol{q})\lambda+F_q,\\ \boldsymbol{A}(\boldsymbol{q})^{\mathrm{T}}\dot{\boldsymbol{q}}&=\boldsymbol{0},\end{aligned}\tag{12}$$

where λ is the Lagrange multiplier, $D(\dot{\boldsymbol{q}})$ is the Rayleigh dissipation function, and F_q is the vector of generalized forcing functions.

In our case, the elements of vectors $\boldsymbol{q}$ and $\dot{\boldsymbol{q}}$ consist of electric charges $q_{\mathrm{C\_PV}}$, $q_{\mathrm{C\_Bat}}$ and $q_{\mathrm{L\_PV}}$, $q_{\mathrm{L\_Bat}}$, q_{O} corresponding to capacitors of the PV and battery DC/DC converters and the inductor of the PV, battery DC/DC converters, and load, respectively.

In the view of the hybrid system configuration presented in Figs. 2–4, we have the following EL equations:

$$T=\frac{1}{2}\left(L_{\mathrm{PV}}\dot{q}_{\mathrm{L\_PV}}^2+L_{\mathrm{Bat}}\dot{q}_{\mathrm{L\_Bat}}^2+L_{\mathrm{O}}\dot{q}_{\mathrm{O}}^2\right),\tag{13}$$

$$V=\frac{1}{2}\left(\frac{1}{C_{\mathrm{PV}}}q_{\mathrm{C\_PV}}^2+\frac{1}{C_{\mathrm{Bat}}}q_{\mathrm{C\_Bat}}^2\right),\tag{14}$$

$$D=\frac{1}{2}r_{\mathrm{PV}}\dot{q}_{\mathrm{L\_PV}}^2+\frac{1}{2}r_{\mathrm{Bat}}\dot{q}_{\mathrm{L\_Bat}}^2+\frac{1}{2}R_{\mathrm{O}}\dot{q}_{\mathrm{O}}^2,\tag{15}$$

$$\boldsymbol{F}=[V_{\mathrm{PV}},\ V_{\mathrm{Bat}},\ 0,\ 0,\ 0]^{\mathrm{T}},\tag{16}$$

where R_{O} and L_{O} are load resistance and inductance, respectively. The constraint equations are given by Kirchhoff's current law, which implies that $\boldsymbol{A}(\boldsymbol{q})$ does not depend on the charge $\boldsymbol{q}$ and thus is a constant $n\times c$ matrix, where c is the number of constraints. Hence, the constraint matrix is

$$\boldsymbol{A}=[1-u_{\mathrm{PV}},\ 1-u_{\mathrm{Bat}},\ -1,\ -1,\ -1]^{\mathrm{T}},\tag{17}$$

with $\boldsymbol{q}$=[$q_{\mathrm{L\_PV}}$, $q_{\mathrm{L\_Bat}}$, q_{O}, $q_{\mathrm{C\_PV}}$, $q_{\mathrm{C\_Bat}}$]$^{\mathrm{T}}$. Considering Eqs. (12) and (17), the EL equations are expanded as a set of scalar differential equations:

$$\frac{\mathrm{d}}{\mathrm{d}t}\left(\frac{\partial L(\dot{\boldsymbol{q}},\boldsymbol{q})}{\partial \dot{q}_{\mathrm{L\_PV}}}\right)-\frac{\partial L(\dot{\boldsymbol{q}},\boldsymbol{q})}{\partial q_{\mathrm{L\_PV}}}=-\frac{\partial D(\dot{\boldsymbol{q}})}{\partial \dot{q}_{\mathrm{L\_PV}}}+(1-u_{\mathrm{PV}})\lambda+V_{\mathrm{PV}},\tag{18}$$

$$\frac{\mathrm{d}}{\mathrm{d}t}\left(\frac{\partial L(\dot{\boldsymbol{q}},\boldsymbol{q})}{\partial \dot{q}_{\mathrm{L\_Bat}}}\right)-\frac{\partial L(\dot{\boldsymbol{q}},\boldsymbol{q})}{\partial q_{\mathrm{L\_Bat}}}=-\frac{\partial D(\dot{\boldsymbol{q}})}{\partial \dot{q}_{\mathrm{L\_Bat}}}+(1-u_{\mathrm{Bat}})\lambda+V_{\mathrm{Bat}},\tag{19}$$

$$\frac{\mathrm{d}}{\mathrm{d}t}\left(\frac{\partial L(\dot{\boldsymbol{q}},\boldsymbol{q})}{\partial \dot{q}_{\mathrm{O}}}\right)-\frac{\partial L(\dot{\boldsymbol{q}},\boldsymbol{q})}{\partial q_{\mathrm{O}}}=-\frac{\partial D(\dot{\boldsymbol{q}})}{\partial \dot{q}_{\mathrm{O}}}-\lambda,\tag{20}$$

$$\frac{\mathrm{d}}{\mathrm{d}t}\left(\frac{\partial L(\dot{\boldsymbol{q}},\boldsymbol{q})}{\partial \dot{q}_{\mathrm{C\_PV}}}\right)-\frac{\partial L(\dot{\boldsymbol{q}},\boldsymbol{q})}{\partial q_{\mathrm{C\_PV}}}=-\frac{\partial D(\dot{\boldsymbol{q}})}{\partial \dot{q}_{\mathrm{C\_PV}}}-\lambda,\tag{21}$$

$$\frac{\mathrm{d}}{\mathrm{d}t}\left(\frac{\partial L(\dot{\boldsymbol{q}},\boldsymbol{q})}{\partial \dot{q}_{\mathrm{C\_Bat}}}\right)-\frac{\partial L(\dot{\boldsymbol{q}},\boldsymbol{q})}{\partial q_{\mathrm{C\_Bat}}}=-\frac{\partial D(\dot{\boldsymbol{q}})}{\partial \dot{q}_{\mathrm{C\_Bat}}}-\lambda.\tag{22}$$

After a straightforward calculation of Eqs. (18)–(22) with the EL parameters given by Eqs. (13)–(17), the EL model equations are yielded in the following form:

$$L_{\mathrm{PV}}\ddot{q}_{\mathrm{L\_PV}}+r_{\mathrm{PV}}\dot{q}_{\mathrm{L\_PV}}+(1-u_{\mathrm{PV}})\lambda=V_{\mathrm{PV}},\tag{23}$$

$$L_{\mathrm{Bat}}\ddot{q}_{\mathrm{L\_Bat}}+r_{\mathrm{Bat}}\dot{q}_{\mathrm{L\_Bat}}+(1-u_{\mathrm{Bat}})\lambda=V_{\mathrm{Bat}},\tag{24}$$

$$L_{\mathrm{O}}\ddot{q}_{\mathrm{L\_O}}+R_{\mathrm{O}}\dot{q}_{\mathrm{L\_O}}+\lambda=0,\tag{25}$$

$$q_{\mathrm{C\_PV}}/C_{\mathrm{PV}}=-\lambda,\tag{26}$$

$$q_{\mathrm{C\_Bat}}/C_{\mathrm{Bat}}=-\lambda.\tag{27}$$

From Eqs. (26) and (27), it is evident that the voltage of the filter capacitor of boost circuits is equal. Therefore, the results with $\boldsymbol{z}=[\dot{q}_{\mathrm{L\_PV}},\ \dot{q}_{\mathrm{L\_Bat}},\ \dot{q}_{\mathrm{L\_O}},\ q_{\mathrm{C\_PV}}/C_{\mathrm{PV}}]$ in the state equation are as follows:

$$L_{\mathrm{PV}}\dot{z}_1+r_{\mathrm{FC}}z_1+(1-u_{\mathrm{PV}})z_4=V_{\mathrm{PV}},\tag{28}$$

$$L_{\mathrm{Bat}}\dot{z}_2+r_{\mathrm{Bat}}z_2+(1-u_{\mathrm{Bat}})z_4=V_{\mathrm{Bat}},\tag{29}$$

$$L_{\mathrm{O}}\dot{z}_3+R_{\mathrm{O}}z_3-z_4=0,\tag{30}$$

$$(C_{\mathrm{PV}}+C_{\mathrm{Bat}})\dot{z}_4-(1-u_{\mathrm{PV}})z_1-(1-u_{\mathrm{Bat}})z_2+z_3=0.\tag{31}$$

The aforementioned equations can be represented in matrix form as

$$\boldsymbol{M}\dot{\boldsymbol{z}}+\boldsymbol{T}(\boldsymbol{u})\boldsymbol{z}+\boldsymbol{R}\boldsymbol{z}=\boldsymbol{E},\tag{32}$$

$$\begin{cases}\boldsymbol{M}=\mathrm{diag}\{L_{\mathrm{PV}},\ L_{\mathrm{Bat}},\ L_{\mathrm{O}},\ C_{\mathrm{PV}}+C_{\mathrm{Bat}}\},\\ \boldsymbol{R}=\mathrm{diag}\{r_{\mathrm{PV}},\ r_{\mathrm{Bat}},\ R_{\mathrm{O}},\ 0\},\\ \boldsymbol{E}=[V_{\mathrm{PV}},\ V_{\mathrm{Bat}},\ 0,\ 0]^{\mathrm{T}},\\ \boldsymbol{T}=\begin{bmatrix}0 & 0 & 0 & 1-u_{\mathrm{PV}}\\ 0 & 0 & 0 & 1-u_{\mathrm{Bat}}\\ 0 & 0 & 0 & -1\\ -(1-u_{\mathrm{PV}}) & -(1-u_{\mathrm{Bat}}) & 1 & 0\end{bmatrix},\end{cases}\tag{33}$$

where $\boldsymbol{M}$ is a positive-definite diagonal matrix, $\boldsymbol{T}$ is the interconnection matrix, $\boldsymbol{R}$ is the dissipation matrix, and $\boldsymbol{E}$ is the vector consisting of voltage sources. The total energy function is

$$H = T + V = \frac{1}{2}\boldsymbol{z}^{\mathrm{T}}\boldsymbol{M}\boldsymbol{z}, \tag{34}$$

where satisfies the energy balance equation

$$H(\gamma) - H(0) + \int_0^{\gamma} \boldsymbol{z}^{\mathrm{T}}\boldsymbol{R}\boldsymbol{z}\mathrm{d}t = \int_0^{\gamma} \boldsymbol{z}^{\mathrm{T}}\boldsymbol{E}\mathrm{d}t, \tag{35}$$

which describes that the sum of the stored energy and dissipated energy equals the supplied energy.

The control objective for this hybrid system is a DC value of the output voltage of both boost DC/DC converters equal to a DC bus constant voltage.

Substitute $z_{4\mathrm{d}}=V_{\mathrm{d}}$ in the dynamic Eqs. (28)–(31). Hence, the equilibrium vector is expressed as

$$\boldsymbol{z}_{\mathrm{d}} = [z_{1\mathrm{d}},\ z_{2\mathrm{d}},\ z_{3\mathrm{d}},\ z_{4\mathrm{d}}]^{\mathrm{T}}, \tag{36}$$

in which $z_{i\mathrm{d}}$ (i=1, 2, 3, 4) denote the desired constant equilibrium points of the closed-loop system.

After some straightforward calculations, the constant value of $z_{3\mathrm{d}}$ is V_{d}/R. From Eqs. (28), (29), and (31) the following equation is achieved:

$$r_{\mathrm{PV}}z_{1\mathrm{d}}^2 + r_{\mathrm{Bat}}z_{2\mathrm{d}}^2 - V_{\mathrm{PV}}z_{1\mathrm{d}} - V_{\mathrm{Bat}}z_{2\mathrm{d}} + V_{\mathrm{d}}^2 / R_{\mathrm{O}} = 0. \tag{37}$$

With a suitable assumption for one of $z_{1\mathrm{d}}$ and $z_{2\mathrm{d}}$ equilibrium points, the other can be achieved from Eq. (37).

5 Passivity-based controller design

In the proposed stand-alone hybrid system, the main objective is the load supplying by only the PV system whenever it has some power generating. Therefore, the DC/DC converter of the PV system is controlled to maintain the DC bus voltage to a constant value. The battery storage has been considered for conditions in which the load power exceeds the generating power of the PV system. Hence, in this condition, the DC bus voltage will be constant with the controlling of the DC/DC converter of battery storage.

5.1 IDA-PBC

Consider the dynamic model of a boost power converter which has been depicted in Fig. 4. The state equations of the converter are

$$\begin{cases} L\dfrac{\mathrm{d}i_{\mathrm{L}}}{\mathrm{d}t} = E_0 - ri_{\mathrm{L}} - (1-u)v_{\mathrm{C}}, \\ C\dfrac{\mathrm{d}v_{\mathrm{C}}}{\mathrm{d}t} = (1-u)i_{\mathrm{L}} - \dfrac{v_{\mathrm{C}}}{R_{\mathrm{O}}}, \end{cases} \tag{38}$$

where u is the continuous output signal which represents the duty cycle of the DC/DC converter, and the positive constants C, L, R_{O}, r, and E_0 are the capacitance, inductance, load resistance, equivalent resistance of the inductor, and voltage source, respectively.

The PCH form of the boost converter is

$$\dot{\boldsymbol{x}} = \big(\boldsymbol{J}(\boldsymbol{x},\boldsymbol{u}) - \boldsymbol{R}(\boldsymbol{x})\big)\frac{\partial H(\boldsymbol{x})}{\partial \boldsymbol{x}} + g(\boldsymbol{x})E, \tag{39}$$

where x_1 is the magnetic flux through the inductor, x_2 is the electrical charge in the capacitor, and

$$\boldsymbol{J} = \begin{bmatrix} 0 & u-1 \\ 1-u & 0 \end{bmatrix},\ \boldsymbol{R} = \begin{bmatrix} r & 0 \\ 0 & 1/R_{\mathrm{O}} \end{bmatrix},\ g(\boldsymbol{x}) = \begin{bmatrix} 1 \\ 0 \end{bmatrix}. \tag{40}$$

Also, $H(\boldsymbol{x})$ is the total energy of the system:

$$H(\boldsymbol{x}) = \frac{1}{2L}x_1^2 + \frac{1}{2C}x_2^2. \tag{41}$$

The equilibrium points for the desired output capacitor voltage V_{d} are given by $\boldsymbol{x}_{\mathrm{d}}=[x_{1\mathrm{d}}, x_{2\mathrm{d}}]^{\mathrm{T}}$ and u_{d}:

$$\begin{gathered} x_{1\mathrm{d}} = \frac{L}{2r}\left(E_0 \pm 2\sqrt{E^2 - \frac{4rV_{\mathrm{d}}^2}{R_{\mathrm{O}}}}\right),\ \ x_{2\mathrm{d}} = CV_{\mathrm{d}}, \\ u_{\mathrm{d}} = 1 - \frac{E_0}{V_{\mathrm{d}}} + \frac{r}{L}\frac{x_{1\mathrm{d}}}{V_{\mathrm{d}}}. \end{gathered} \tag{42}$$

It is evident that u_{d} is not constant, but depends on $x_{1\mathrm{d}}$. Therefore, u_{d} depends on load resistance.

Consider the injected damping matrix as

$$\boldsymbol{R}_{\mathrm{a}} = \mathrm{diag}\{-r + R_{\mathrm{a}},\ -1/R_{\mathrm{O}}\},\ \ R_{\mathrm{a}} > 0.$$

Assuming $u=\beta(x_2)$ and $\boldsymbol{J}_a(\boldsymbol{x})=\boldsymbol{0}$, to simplify the process of solving the PDE (6), define

$$\boldsymbol{K}(\boldsymbol{x})=\begin{bmatrix}K_1 & K_2\end{bmatrix}^{\mathrm{T}}=\frac{\partial H_a(\boldsymbol{x})}{\partial \boldsymbol{x}}.$$

Then

$$\begin{bmatrix}-R_a & u-1\\ 1-u & 0\end{bmatrix}\begin{bmatrix}K_1\\ K_2\end{bmatrix}=\begin{bmatrix}R_a-r & 0\\ 0 & -\dfrac{1}{R_O}\end{bmatrix}\begin{bmatrix}\dfrac{1}{L}x_1\\ \dfrac{1}{C}x_2\end{bmatrix}+\begin{bmatrix}1\\ 0\end{bmatrix}E, \tag{43}$$

$$\boldsymbol{K}=\begin{bmatrix}-\dfrac{x_2}{R_OC(1-\beta(x_2))}\\ \dfrac{R_ax_2}{R_OC(1-\beta(x_2))^2}-\dfrac{x_1(R_a-r)/L+E_0}{1-\beta(x_2)}\end{bmatrix}.$$

As β is a function only of x_2, the integrability condition Eq. (8) reduces to the simple ODE:

$$\frac{\partial K_2(\boldsymbol{x})}{\partial x_1}=\frac{\partial K_1(\boldsymbol{x})}{\partial x_2},$$

$$-\frac{R_a-r}{L\left(1-\beta(x_2)\right)}=-\frac{x_2\beta(x_2)}{RC\left(1-\beta(x_2)\right)^2}-\frac{1}{RC\left(1-\beta(x_2)\right)}, \tag{44}$$

which can be easily solved by the separation of the variables method to obtain u.

$$\frac{x_2\dot{\beta}(x_2)}{1-\beta(x_2)}=-\left(1-\frac{RC}{L}(R_a-r)\right). \tag{45}$$

Defining $\alpha\triangleq 1-RC(R_a-r)/L$, the controller will be

$$u=1-c_1x_2^{\alpha}, \tag{46}$$

where c_1 is a constant which is chosen to assign the equilibrium condition Eq. (9):

$$\left.\frac{\partial H_d}{\partial x}\right|_{x=x_2}=\left.\left(\frac{\partial H}{\partial x}+\frac{\partial H_a}{\partial x}\right)\right|_{x=x_2}=0. \tag{47}$$

This yields $c_1=(1-u_d)/(CV_d)^{\alpha}$. Hence, the IDA-PB controller of the boost converter is

$$u=1-(1-u_d)(x_2/x_{2d})^{\alpha}. \tag{48}$$

5.2 EL-PBC design

In this subsection, the EL-PB controllers are designed based on Eq. (33). Consider the error state vector

$$\begin{aligned}\tilde{\boldsymbol{z}}&=[z_{1d},\ z_{2d},\ z_{3d},\ z_{4d}]^{\mathrm{T}}\\ &=[z_1-z_{1d},\ z_2-z_{2d},\ z_3-z_{3d},\ z_4-z_{4d}]^{\mathrm{T}}.\end{aligned}$$

The error dynamic equation is expressed as

$$\boldsymbol{M}\dot{\tilde{\boldsymbol{z}}}+\boldsymbol{T}(\boldsymbol{u})\tilde{\boldsymbol{z}}+\boldsymbol{R}\tilde{\boldsymbol{z}}=\boldsymbol{E}-(\boldsymbol{M}\dot{\boldsymbol{z}}_d+\boldsymbol{T}\boldsymbol{z}_d+\boldsymbol{R}\boldsymbol{z}_d). \tag{49}$$

Adding $\boldsymbol{R}_a\tilde{\boldsymbol{z}}$ to both sides of Eq. (49), the error dynamics with desired damping is

$$\boldsymbol{M}\dot{\tilde{\boldsymbol{z}}}+\boldsymbol{T}(\boldsymbol{u})\tilde{\boldsymbol{z}}+\boldsymbol{R}\tilde{\boldsymbol{z}}=\boldsymbol{E}-(\boldsymbol{M}\dot{\boldsymbol{z}}_d+\boldsymbol{T}\boldsymbol{z}_d+\boldsymbol{R}\boldsymbol{z}_d-\boldsymbol{R}_a\tilde{\boldsymbol{z}}). \tag{50}$$

Consider the following desired error dissipation matrix:

$$\boldsymbol{R}_d=\boldsymbol{R}+\boldsymbol{R}_a, \tag{51}$$

where

$$\boldsymbol{R}_a=\mathrm{diag}\{r_{a1},\ r_{a2},\ 0,\ 0\}. \tag{52}$$

Suppose the right-hand side of Eq. (50) is zero, i.e.,

$$\boldsymbol{M}\dot{\tilde{\boldsymbol{z}}}+\boldsymbol{T}(\boldsymbol{u})\tilde{\boldsymbol{z}}+\boldsymbol{R}\tilde{\boldsymbol{z}}=\boldsymbol{0}. \tag{53}$$

Consider the total energy, $H=0.5\boldsymbol{z}^{\mathrm{T}}\boldsymbol{M}\boldsymbol{z}$, as a Lyapunov function. For Eq. (53) the asymptotic stability of the error dynamics is achieved due to the positive definiteness of matrix $\boldsymbol{M}$ and satisfying its derivative

$$\dot{H}_d(t)=-\tilde{\boldsymbol{z}}^{\mathrm{T}}\boldsymbol{R}_d\boldsymbol{z}\le 0,\quad \forall\tilde{\boldsymbol{z}}\ne\boldsymbol{0}. \tag{54}$$

It is concluded that the error dynamics Eq. (53) is asymptotically stable to zero.

Thus, to obtain desired error dynamics Eq. (53), compare Eq. (50) and Eq. (53):

$$\boldsymbol{M}\dot{\boldsymbol{z}}_d+\boldsymbol{T}(\boldsymbol{u})\boldsymbol{z}_d+\boldsymbol{R}\boldsymbol{z}_d-\boldsymbol{R}_a\tilde{\boldsymbol{z}}=\boldsymbol{E}. \tag{55}$$

The above equation is extended to the following scalar differential equations:

$$L_{PV}\dot{z}_{1d}+r_{PV}z_{1d}+(1-u_{PV})z_{4d}-r_{a1}(z_1-z_{1d})=V_{PV}, \tag{56}$$

$$L_{Bat}\dot{z}_{2d}+r_{Bat}z_{2d}+(1-u_{Bat})z_{4d}-r_{a2}(z_2-z_{2d})=V_{Bat}, \tag{57}$$

$$L_{\mathrm{O}}\dot{z}_{3\mathrm{d}}+R_{\mathrm{O}}z_{3\mathrm{d}}-z_{4\mathrm{d}}=0, \tag{58}$$

$$(C_{\mathrm{PV}}+C_{\mathrm{Bat}})\dot{z}_{4\mathrm{d}}-(1-u_{\mathrm{PV}})z_{1\mathrm{d}}-(1-u_{\mathrm{Bat}})z_{2\mathrm{d}}+z_{3\mathrm{d}}=0. \tag{59}$$

In this work, the control objective is the PBC of DC output voltage, but the direct control is not feasible due to its lack of stability (Escobar *et al*., 1999). Hence, the indirect control is used for the regulation of the output DC voltage to a constant equilibrium value.

Consider the equations of the boost DC/DC converter of the PV system (56) and (59). The desired constant value for the PV current (converter input current) is $z_{1\mathrm{d}}$. From Eq. (56), the control variable u_{PV} can be solved as

$$u_{\mathrm{PV}}=1-\left[V_{\mathrm{PV}}-r_{\mathrm{PV}}z_{1\mathrm{d}}+r_{\mathrm{a}1}(z_1-z_{1\mathrm{d}})\right]/z_{4\mathrm{d}}. \tag{60}$$

Also, consider the equations of the DC/DC converter of battery storage Eqs. (56) and (59). The desired constant value for the battery current is $z_{2\mathrm{d}}$, and the control variable u_{Bat} can be solved from Eq. (57) as

$$u_{\mathrm{Bat}}=1-\left[V_{\mathrm{Bat}}-r_{\mathrm{Bat}}z_{2\mathrm{d}}+r_{\mathrm{a}2}(z_2-z_{2\mathrm{d}})\right]/z_{4\mathrm{d}}. \tag{61}$$

Substituting Eqs. (60) and (61) into Eq. (59), after a straightforward calculation, the controller state, $z_{4\mathrm{d}}$, can be achieved as

$$\dot{z}_{4\mathrm{d}}=\frac{1}{C_{\mathrm{PV}}+C_{\mathrm{Bat}}}\left[\frac{z_{1\mathrm{d}}}{z_{4\mathrm{d}}}\left(V_{\mathrm{PV}}-r_{\mathrm{PV}}z_{1\mathrm{d}}+r_{\mathrm{a}1}(z_1-z_{1\mathrm{d}})\right)+\frac{z_{2\mathrm{d}}}{z_{4\mathrm{d}}}\left(V_{\mathrm{Bat}}-r_{\mathrm{Bat}}z_{2\mathrm{d}}+r_{\mathrm{a}2}(z_2-z_{2\mathrm{d}})\right)-z_{3\mathrm{d}}\right]. \tag{62}$$

Calculation of the controller state $z_{4\mathrm{d}}$ depends on $z_{3\mathrm{d}}$, which can be achieved as

$$z_{3\mathrm{d}}=(z_{4\mathrm{d}}-Rz_4)/L_{\mathrm{O}}. \tag{63}$$

6 Power management system

In the proposed hybrid DC power source, the PV system and the battery storage have cooperation to supply the load. Hence, the power management system (PMS) needs to control the power flow among the PV system, battery storage, and the load.

The PMS acts based on certain strategies. In this study, the PMS strategies have been considered as the following:

1. The PV is the main source to supply power to the load.

2. The battery storage is a secondary source to supply load when either the PV system has not any power generation or the load is more than the generated power of the PV system.

3. The battery storage is charged by the PV when the load power is lower than the generated power of the PV system.

According to the abovementioned strategies, the PMS algorithm is as shown in Fig. 5.

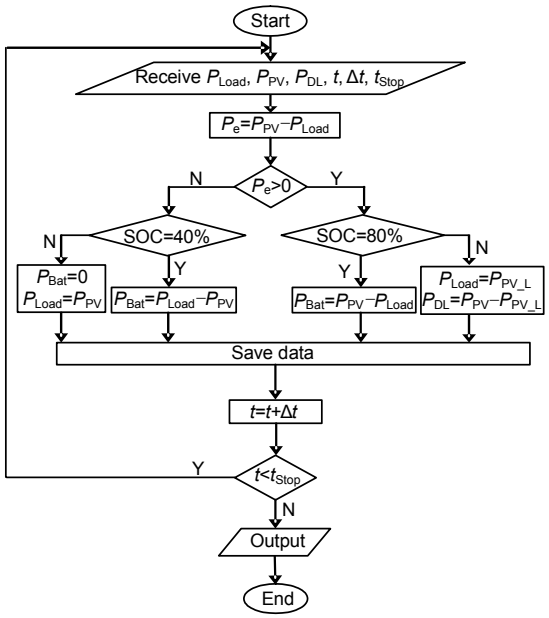

Fig. 5 Flowchart of the proposed power management system

7 Simulation results and discussion

The purpose of this study is to address the port-controlled Hamiltonian and EL framework modeling and PBC of a stand-alone PV/battery hybrid power source. MATLAB/Simulink environment is used to investigate the performance of the PBC on the PV/battery hybrid power source. The mathematical model of each component in the DC hybrid power source has been presented in the previous sections. It consists of the model of the PV cell in which the related parameters have been calculated based on the Walker model (Walker, 2001), the dynamic model of

Li-ion battery, the nonlinear model of the DC/DC boost converter and bidirectional DC/DC converter, the dump load consisting of resistors connected in series with switches (Sebastian and Quesada, 2006), PB controllers, and the PMS. The Simulink model of the converters and controllers is illustrated in Fig. 6. Table 1 shows the specifications of the PV system, which consists of a combination of two modules in parallel and four modules in series. The specifications of the Li-ion battery storage are given in Table 2. The DC/DC converter specifications are given in Table 3.

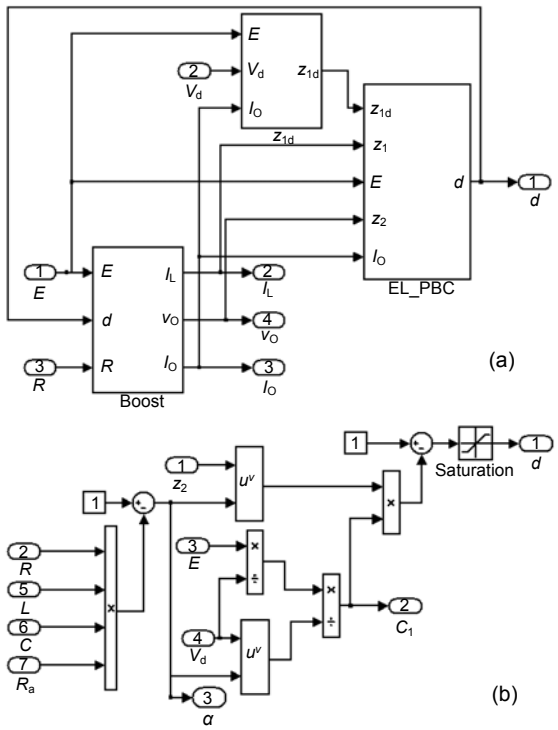

Fig. 6 Simulink models: (a) Euler-Lagrange passivity-based control (EL-PBC) and boost converter; (b) interconnection and damping assignment passivity-based control (IDA-PBC)

Table 1 Specifications of the BP 485J photovoltaic module*

Parameter	Value	Parameter	Value
Maximum power (W)	85	Open circuit voltage (V)	22.2
Voltage at MPP (V)	17.8	Module efficiency	13.1%
Current at MPP (A)	4.8	Number of modules in series	4
Short circuit current (A)	5.1	Number of strings in parallel	2

* Specifications of 85 W photovoltaic module, http://www.amerecoslar.com/SolarSite/ProductsAndSolutions/SolarPanels/BPSolar/85WattPanel.aspx. MPP: maximum power point

Table 2 Specifications of Li-ion battery*

Parameter	Value
Capacity (mA·h)	850
Nominal voltage (V)	3.7
Maximum charge voltage (V)	4.23
Number of series cells	11
Number of parallel strings	8

* Specifications of polymer lithium ion battery, model: PL-383562

Table 3 Specifications of DC/DC converters

Parameter	Value	Parameter	Value
L_{PV} (mH)	23.2	L_{Bat} (mH)	100
C_{PV} (μF)	330	C_{Bat} (μF)	87
r_{PV} (Ω)	0.03	r_{Bat} (Ω)	0.07

Our simulations are achieved in two cases: (1) the initial SOC of the battery storage is 70%; (2) the initial SOC of battery storage is 85%.

The rated power of the PV system is 680 W; the solar irradiance is the same for these two cases (Fig. 7a). The load consists of series combination of inductance (L=10 mH) and resistance (Fig. 7b). The DC bus voltage reference is 100 V.

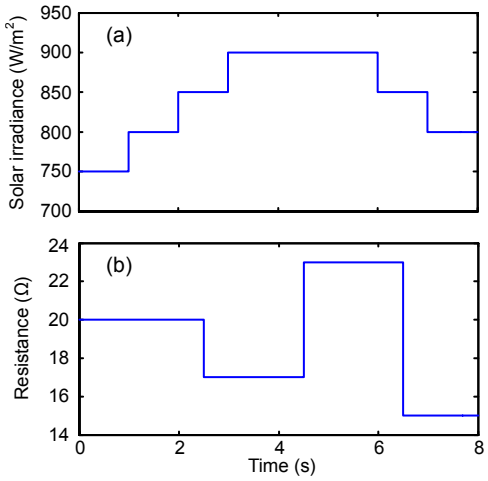

Fig. 7 Solar irradiance (a) and load resistance (b)

7.1 First case

Variance of load resistance occurs on three stages at 2.5, 4.5, and 6.5 s. The load voltage (V_{DC}) and current (I_O) are shown in Fig. 8. It is evident that the PB controllers exhibit a smooth and fast transient to a step change in the load resistance, and particularly the solar irradiance. The comparison of load voltage and current based on both types of PB

controllers demonstrates to this fact that the IDA-PBC does not have a zero steady-state error, but the steady-state error of the EL-PBC, which is 1.5 V, is clear in Fig. 8a (t=4.5 s). Also, the overshoot of the IDA-PBC is higher than that of the EL-PBC.

Fig. 9 shows the PV system voltage (V_{PV}) and current (I_{PV}). These are obtained based on the P&O MPPT algorithm.

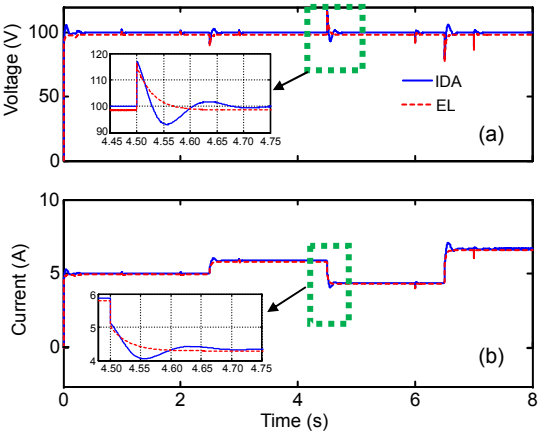

Fig. 8 Variation of load voltage (a) and current (b)

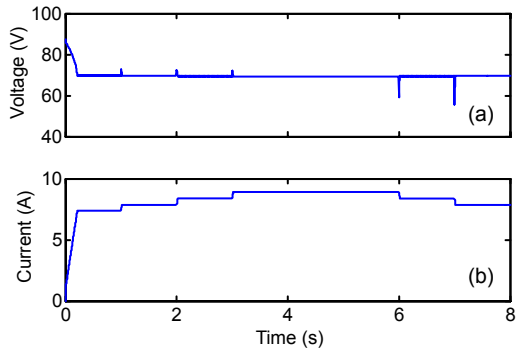

Fig. 9 PV system voltage (a) and current (b) at the maximum power point

The battery storage voltage (V_{Bat}) and current (I_{Bat}) under the change of solar irradiance and load resistance are shown in Fig. 10. The battery voltage and current based on EL-PBC have less overshoot than those based on IDA-PBC, but the steady-state error of load voltage and current based on EL-PBC demonstrates itself on the voltage and current of battery storage, which is evident from Figs. 10a and 10b.

Fig. 10c presents the SOC of the battery storage to demonstrate the charge and discharge modes. In this case, the initial SOC of the battery storage is 70%. Therefore, the battery storage is in the discharge mode between 6.5 s and 8 s. Moreover, the load power exceeds the generated power of the PV system, which is evident from Fig. 11.

Fig. 11 shows the power flow among hybrid power source components based on both controllers. The EL-PBC (Fig. 11b) settles to the steady-state value faster than IDA-PBC (Fig. 11a), but it has a steady-state error which differs from those from the delivered power of load with IDA-PBC.

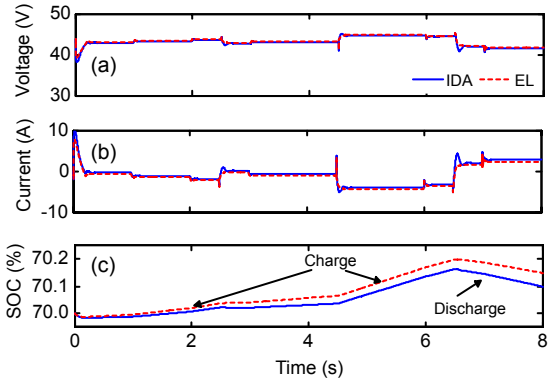

Fig. 10 Variation of battery storage voltage (a), current (b), and SOC (c)

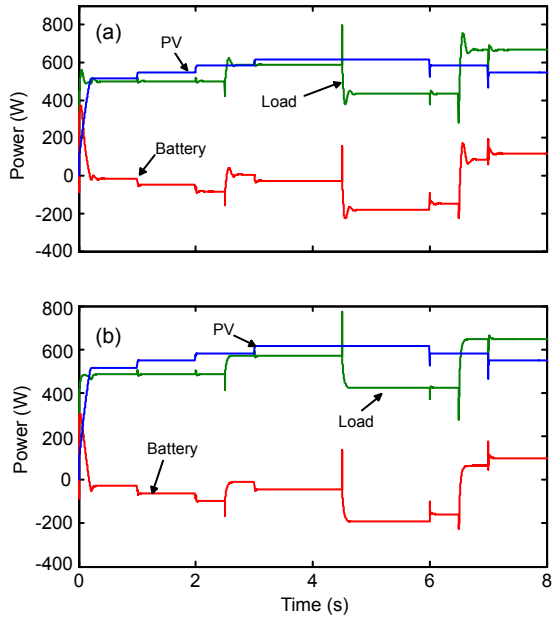

Fig. 11 Variation of load, PV, and battery storage power: (a) interconnection and damping assignment passivity-based control (IDA-PBC); (b) Euler-Lagrange passivity-based control (EL-PBC)

Control signals of the DC/DC converters of the PV system and the battery storage are presented in

Fig. 12. In this case, the DC load supplied by the hybrid power source based on the EL-PBC has a low overshoot and short settling time towards the IDA-PBC.

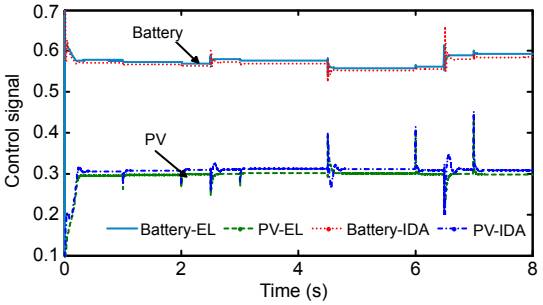

Fig. 12 Control signals of DC/DC converters

7.2 Second case

In the second case, the initial SOC of battery storage is 85%. It is out of the range that has been defined on the PMS strategies. In other words, it is not in the safest charge mode in this case.

Fig. 13 presents the battery storage voltage and current based on both types of PB controllers. According to Figs. 13a and 13b, the voltage and current of battery storage have fluctuations whenever the load resistance changes or the other transient condition occurs. In Fig. 13c, the SOC illustrates to discharge of battery storage that occurs between 6.5 s and 8 s.

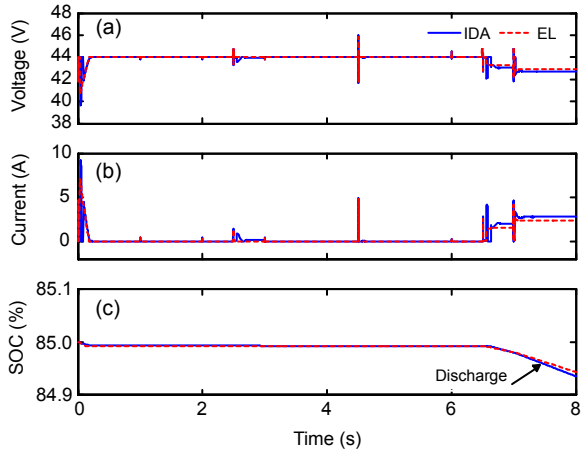

Fig. 13 Variation of battery storage voltage (a), current (b), and SOC (c)

Considering the battery storage limitations, whenever the power generated by the PV system exceeds the load power, the dump load consumes excess power from the PV system (Fig. 14). The power consumed by dump load is variable; its value is specified by PMS strategies between 0.2 s and 6.5 s.

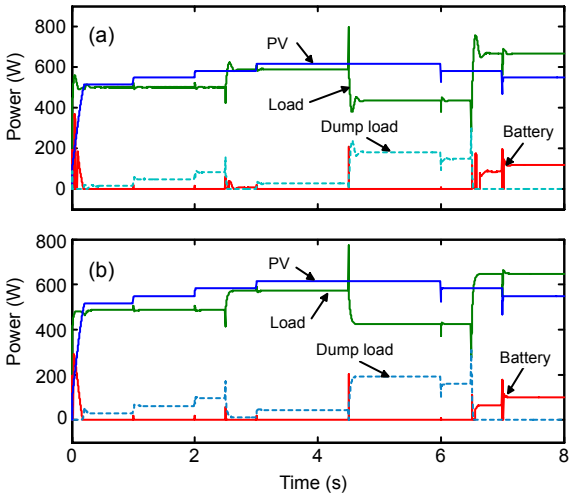

Fig. 14 Variation of load, PV, dump load, and battery storage power: (a) interconnection and damping assignment passivity-based control (IDA-PBC); (b) Euler-Lagrange passivity-based control (EL-PBC)

The comparison of Figs. 14a and 14b demonstrates that, the steady-state error of IDA-PBC is zero but there is considerable error for EL-PBC. The advantages of EL-PBC towards IDA-PBC are shorter settling time and lower overshoot.

It is evident that the hybrid power source with the proposed controllers is more reasonable towards the solar irradiance and the load resistance changes. The IDA-PBC and EL-PBC have some advantages and disadvantages with respect to each other, as have been presented in the above explanations.

8 Conclusions

A stand-alone hybrid PV/battery power source and the power electronic interface based on port-controlled Hamiltonian systems and Euler-Lagrange framework have been modeled. Corresponding to the method of modeling, the PB controllers have been designed. The PV system, battery storage, and load constraints have been considered to manage power flow between them.

The proposed hybrid PV/battery power source exhibits excellent performance for the load resistance and solar irradiance changes. To investigate the

validity of the proposed system, two cases have been simulated based on SOC of battery storage. The battery storage, based on the load power situation, has cooperation to supply power to the load and absorb power from the PV system in the first case where SOC is 70%. But in the second case where SOC is 85%, the battery storage only supplies power to the load. The remaining power of the PV system is consumed by the dump load.

The results of the proposed hybrid system in both cases demonstrate that the EL-PBC has a lower overshoot and a shorter settling time towards the IDA-PBC. In contrast, the steady-state error of IDA-PBC is zero, but there is considerable error for EL-PBC.

References

Ayad, M.Y., Becherif, M., Henni, A., Aboubou, A., Wack, M., Laghrouche, S., 2010. Passivity-based control applied to DC hybrid power source using fuel cell and supercapacitors. *Energy Conv. Manag.*, **51**(7):1468-1475. [doi:10.1016/j.enconman.2010.01.023]

Becherif, M., Paire, D., Miraoui, A., 2007. Energy Management of Solar Panel and Battery System with Passive Control. Int. Conf. on Clean Electrical Power, p.14-19. [doi:10.1109/ICCEP.2007.384179]

Carrasco, J.M., Franquelo, L.G., Bialasiewicz, J.T., Galván, E., Guisado, R.C.P., Prats, M.Á.M., León, J.I., Moreno-Alfonso, N., 2006. Power-electronic systems for the grid integration of renewable energy sources: a survey. *IEEE Trans. Ind. Electron.*, **53**(4):1002-1016. [doi:10.1109/TIE.2006.878356]

Chen, M., Rincon-Mora, G.A., 2006. Accurate electrical battery model capable of predicting runtime and *I–V* performance. *IEEE Trans. Energy Conv.*, **21**(2):504-511. [doi:10.1109/TEC.2006.874229]

Dali, M., Belhadj, J., Roboam, X., 2010. Hybrid solar–wind system with battery storage operating in grid-connected and standalone mode: control and energy management—experimental investigation. *Energy*, **35**(6):2587-2595. [doi:10.1016/j.energy.2010.03.005]

Dalsmo, M., van der Schaft, A., 1998. On representations and integrability of mathematical structures in energy-conserving physical systems. *SIAM J. Control Optim.*, **37**(1):54-91. [doi:10.1137/S0363012996312039]

Dòria-Cerezo, A., 2006. Modeling, Simulation and Control of a Doubly-Fed Induction Machine Controlled by a Back-to-Back Converter. PhD Thesis, Technical University of Catalonia, Spain.

Durr, M., Cruden, A., Gair, S., McDonald, J.R., 2006. Dynamic model of a lead acid battery for use in a domestic fuel cell system. *J. Power Sources*, **161**(2):1400-1411. [doi:10.1016/j.jpowsour.2005.12.075]

Duryea, S., Isalm, S., Lawrance, W., 2001. A battery management system for stand-alone photovoltaic energy systems. *IEEE Ind. Appl. Mag.*, **7**(3):67-72. [doi:10.1109/2943.922452]

El-Shatter, T.F., Eskander, M.N., El-Hagry, M.T., 2006. Energy flow and management of a hybrid wind/PV/fuel cell generation system. *Energy Conv. Manag.*, **47**(9-10):1264-1280. [doi:10.1016/j.enconman.2005.06.022]

Escobar, G., Ortega, R., Sira-Ramirez, H., Vilain, J.P., Zein, I., 1999. An experimental comparison of several nonlinear controllers for power converters. *IEEE Control Syst. Mag.*, **19**(1):66-82. [doi:10.1109/37.745771]

Esram, T., Chapman, P.L., 2007. Comparison of photovoltaic array maximum power point tracking techniques. *IEEE Trans. Energy Conv.*, **22**(2):439-449. [doi:10.1109/TEC.2006.874230]

Glavin, M.E., Chan, P.K.W., Armstrong, S., Hurley, W.G., 2008. A Stand-Alone Photovoltaic Supercapacitor Battery Hybrid Energy Storage System. 13th Int. Power Electronics and Motion Control Conf., p.1688-1695. [doi:10.1109/EPEPEMC.2008.4635510]

Golkar, M.A., Hajizadeh, A., 2009. Control strategy of hybrid fuel cell/battery distributed generation system for grid-connected operation. *J. Zhejiang Univ.-Sci. A*, **10**(4):488-496. [doi:10.1631/jzus.A0820151]

Jeong, K.S., Lee, W.Y., Kim, C.S., 2005. Energy management strategies of a fuel cell/battery hybrid system using fuzzy logics. *J. Power Sources*, **145**(2):319-326. [doi:10.1016/j.jpowsour.2005.01.076]

Jiang, Z., Gao, L., Dougal, R.A., 2007. Adaptive control strategy for active power sharing in hybrid fuel cell/battery power sources. *IEEE Trans. Energy Conv.*, **22**(2):507-515. [doi:10.1109/TEC.2005.853747]

Khateeb, S.A., Farid, M.M., Selman, J.R., Al-Hallaj, S., 2006. Mechanical–electrochemical modeling of Li-ion battery designed for an electric scooter. *J. Power Sources*, **158**(1):673-678. [doi:10.1016/j.jpowsour.2005.09.059]

Kim, D.E., Lee, D.C., 2007. Feedback Linearization Control of Three-Phase AC/DC PWM Converters with LCL Input Filters. 7th Int. Conf. on Power Electronics, p.766-771. [doi:10.1109/ICPE.2007.4692491]

Kim, I.S., Kim, M.B., Youn, M.J., 2006. New maximum power point tracker using sliding-mode observer for estimation of solar array current in the grid-connected photovoltaic system. *IEEE Trans. Ind. Electron.*, **53**(4):1027-1035. [doi:10.1109/TIE.2006.878331]

Komurcugil, H., 2010. Steady-state analysis and passivity-based control of single-phase PWM current-source inverters. *IEEE Trans. Ind. Electron.*, **57**(3):1026-1030. [doi:10.1109/TIE.2009.2025297]

Koutroulis, E., Kalaitzakis, K., Voulgaris, N.C., 2001. Development of a microcontroller based, photovoltaic maximum power point tracking control system. *IEEE Trans. Power Electron.*, **16**(1):46-54. [doi:10.1109/63.903988]

Kwasinski, A., Krein, P.T., 2007. Passivity-Based Control of Buck Converters with Constant-Power Loads. IEEE Power Electronics Specialists Conf., p.259-265. [doi:10.1109/PESC.2007.4341998]

Kwon, J.M., Nam, K.H., Kwon, B.H., 2006. Photovoltaic power conditioning system with line connection. *IEEE Trans. Ind. Electron.*, **53**(4):1048-1054. [doi:10.1109/TIE.2006.878329]

Kwon, J.M., Kwon, B.H., Nam, K.H., 2008. Three-phase photovoltaic system with three-level boosting MPPT control. *IEEE Trans. Power Electron.*, **23**(5):2319-2327. [doi:10.1109/TPEL.2008.2001906]

Lagorse, J., Paire, D., Miraoui, A., 2009. Sizing optimization of a stand-alone street lighting system powered by a hybrid system using fuel cell, PV and battery. *Renew. Energy*, **34**(3):683-691. [doi:10.1016/j.renene.2008.05.030]

Lee, T.S., 2004. Lagrangian modeling and passivity-based control of three-phase AC/DC voltage-source converters. *IEEE Trans. Ind. Electron.*, **51**(4):892-902. [doi:10.1109/TIE.2004.831753]

Leyva, R., Cid-Pastor, A., Alonso, C., Queinnec, I., Tarbouriech, S., Martinez-Salamero, L., 2006. Passivity-based integral control of a boost converter for large-signal stability. *IEE Proc.-Control Theory Appl.*, **153**(2):139-146. [doi:10.1049/ip-cta:20045223]

Lu, D.D.C., Agelidis, V.G., 2009. Photovoltaic-battery-powered DC bus system for common portable electronic devices. *IEEE Trans. Power Electron.*, **24**(3):849-855. [doi:10.1109/TPEL.2008.2011131]

Márquez-Contreras, R., Rodríguez-Cortés, H., Spinetti-Rivera, M., 2008. Revisiting IDA-PBC, Open-Loop Control, and Modeling for the Boost DC-DC Power Converter. Latin American Congress of Automatic Control.

Mazumder, S.K., Nayfeh, A.H., Borojevic, D., 2002. Robust control of parallel DC–DC buck converters by combining integral-variable-structure and multiple-sliding-surface control schemes. *IEEE Trans. Power Electron.*, **17**(3):428-437. [doi:10.1109/TPEL.2002.1004251]

Moreno, J., Ortúzar, M.E., Dixon, J.W., 2006. Energy-management system for a hybrid electric vehicle, using ultracapacitors and neural networks. *IEEE Trans. Ind. Electron.*, **53**(2):614-623. [doi:10.1109/TIE.2006.870880]

Ortega, R., Loria, A., Nicklasson, P.J., Sira-Ramirez, H., 1998. Passivity Based Control of Euler-Lagrange Systems: Mechanical, Electrical and Electrochemical Applications. Springer-Verlag, London, UK.

Ortega, R., van der Schaft, A., Maschke, B., Escobar, G., 2002. Interconnection and damping assignment passivity-based control of port-controlled Hamiltonian systems. *Automatica*, **38**(4):585-596. [doi:10.1016/S0005-1098(01)00278-3]

Scarpa, V., Buso, S., Spiazzi, G., 2009. Low-complexity MPPT technique exploiting the PV module MPP locus characterization. *IEEE Trans. Ind. Electron.*, **56**(5):1531-1538. [doi:10.1109/TIE.2008.2009618]

Scherpen, J.M.A., Jeltsema, D., Klaassens, J.B., 2003. Lagrangian modeling of switching electrical networks. *Syst. Control Lett.*, **48**(5):365-374. [doi:10.1016/S0167-6911(02)00290-6]

Sebastian, R., Quesada, J., 2006. Distributed control system for frequency control in an isolated wind system. *Renew. Energy*, **31**(3):285-305. [doi:10.1016/j.renene.2005.04.003]

Sera, D., Kerekes, T., Teodorescu, R., Blaabjerg, F., 2006. Improved MPPT Algorithms for Rapidly Changing Environmental Conditions. 12th Int. Conf. on Power Electronics and Motion Control, p.1614-1619. [doi:10.1109/EPEPEMC.2006.4778635]

Sira-Ramirez, H., Ortega, R., Garcia-Esteban, M., 1998. Adaptive passivity-based control of average DC-to-DC power converter models. *Int. J. Adapt. Control Signal Process.*, **12**(1):63-80. [doi:10.1002/(SICI)1099-1115(199802)12:1<63::AID-ACS467>3.0.CO;2-#]

Timbus, A., Liserre, M., Teodorescu, R., Rodriguez, P., Blaabjerg, F., 2009. Evaluation of current controllers for distributed power generation systems. *IEEE Trans. Power Electron.*, **24**(3):654-664. [doi:10.1109/TPEL.2009.2012527]

Uzunoglu, M., Onar, O.C., Alam, M.S., 2009. Modeling, control and simulation of a PV/FC/UC based hybrid power generation system for stand-alone applications. *Renew. Energy*, **34**(3):509-520. [doi:10.1016/j.renene.2008.06.009]

Vmquez, N., Hernandez, C., Alvarez, J., Arau, J., 2003. Sliding Mode Control for DC/DC Converters: a New Sliding Surface. Int. Symp. on Industrial Electronics, p.422-426.

Walker, G., 2001. Evaluating MPPT converter topologies using a Matlab PV model. *J. Electr. Electron. Eng. Aust.*, **21**(1):49-56.

Wang, P., Wang, J., Xu, Z., 2008. Passivity-Based Control of Three Phase Voltage Source PWM Rectifiers Based on PCHD Model. Int. Conf. on Electrical Machines and Systems, p.1126-1130.

Wang, Z., Chang, L., 2008. A DC voltage monitoring and control method for three-phase grid-connected wind turbine inverters. *IEEE Trans. Power Electron.*, **23**(3):1118-1125. [doi:10.1109/TPEL.2008.921174]

Yu, D., Yuvarajan, S., 2006. Load Sharing in a Hybrid Power Source with a PV Panel and PEM Fuel-Cell. 21st Annual IEEE Conf. and Exposition on Applied Power Electronics, p.1245-1249. [doi:10.1109/APEC.2006.1620698]